

Local structure of ReO_3 at ambient pressure from neutron total scattering study

E. S. Božin,¹ T. Chatterji,² and S. J. L. Billinge^{1,3}

¹*Department of Condensed Matter Physics and Materials Science,
Brookhaven National Laboratory, Upton, NY 11973, USA*

²*Institut Laue-Langevin, 6 rue Jules Horowitz, BP 156 Grenoble cedex 9, France and*

³*Department of Applied Physics and Applied Mathematics,
Columbia University, New York, NY 10027, USA*

(Dated: July 2, 2012)

A hypothesis that the local rotations of ReO_6 octahedra persist in the crystallographically untitled ambient phase of ReO_3 is examined by the high-resolution neutron time-of-flight total scattering based atomic pair distribution function analysis. Three candidate models were tested, $\text{Pm}\bar{3}\text{m}$, $\text{P4}/\text{mbm}$, and $\text{Im}\bar{3}$, for the local structure of ReO_3 at ambient pressure and 12 K, and both quantitative and qualitative assessment of the data were performed. No evidence for large local octahedral rotations was found, suggesting that the local and the average structure are the same ($\text{Pm}\bar{3}\text{m}$) as normally assumed.

PACS numbers: 61.05.F, 62.50.-p, 81.05.Je, 91.55.Nc

I. INTRODUCTION

Among d-electron metallic conductors ReO_3 has a simple perovskite-like structure and its conductivity is comparable to that of a noble metal such as Ag.^{1,2} Although the electron-phonon coupling constant is not very small, ReO_3 surprisingly does not show superconductivity down to 20 mK.³ ReO_3 seems to belong to the normal class of conventional band Fermi liquids with electron-phonon interaction dominating the resistivity.³

ReO_3 crystallizes in the cubic space group $\text{Pm}\bar{3}\text{m}$ with the undistorted perovskite-like DO_9 type structure (ABO_3 , Fig. 1) comprised of a network of corner-shared ReO_6 octahedra and with an empty A-site, and is in fact the simplest material containing BO_6 octahedra. ReO_3 is very special among the multitude of systems possessing the perovskite-based structure, in that its untitled cubic $\text{Pm}\bar{3}\text{m}$ structure is extremely stable at ambient pressure

and at all temperatures from liquid-helium temperature⁴ up to its melting point at 673 K.^{5,6} Electronic band structure calculations investigated this extraordinary structural stability⁶ and suggested that metallic bonding plays an important role.⁷ The open crystal structure makes ReO_3 suitable for doping or compression under high-pressure. ReO_3 attracted considerable attention recently due to observation of weak negative thermal expansion (NTE) below room temperature.⁸ NTE is rarely found in metals, and in ReO_3 is rather sensitive to impurity induced disorder.⁹

A structural phase transition was discovered in ReO_3 upon application of pressure when the pressure induced anomaly in the Fermi surface was observed in measurements of De Haas-van Alphen frequencies,¹⁰ and was characterized in detail by means of x-ray and neutron diffraction.^{11–13} At room temperature ReO_3 undergoes a pressure-induced second order phase transition at $p_c = 5.2 \text{ kbar}$, to an intermediate tetragonal phase ($\text{P4}/\text{mbm}$) over a narrow pressure range, and further to a cubic ($\text{Im}\bar{3}$) phase that persists up to relatively high pressures while the ReO_6 octahedra remain almost undistorted,¹⁴ but considerably tilted.¹⁵ The driving force for the transition is argued to be the softening of the M3 phonon mode involving a rigid rotation of ReO_6 octahedra. It is a continuous transition with the rotation angle as an order parameter.¹³ The pressure-temperature phase diagram has been recently established,¹⁶ indicating that value of p_c decreases with decreasing temperature, leveling at around 2.4 kbar at base temperature. More recently, a study of the pressure induced phase transition showed that in nanocrystalline ReO_3 , the sequence of phases is different and with generally lower p_c values than for bulk samples.¹⁷

This canonical view has been challenged by the reexamination¹⁸ of the structural phase transition in ReO_3 using the x-ray absorption fine structure (XAFS) method sensitive to the nearest neighbor information. This investigation suggests that even at ambient pressure the Re-

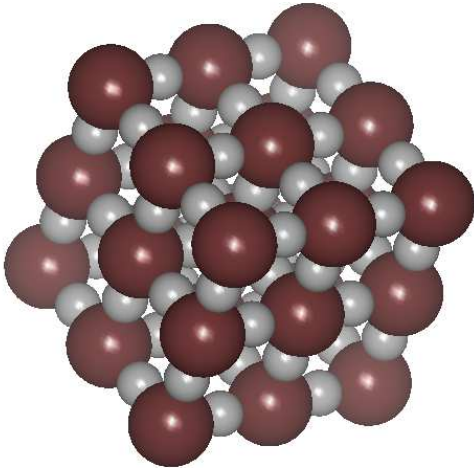


FIG. 1: Structural motif of ReO_3 (space group $\text{Pm}\bar{3}\text{m}$): Re is shown as large spheres, while small spheres represent O.

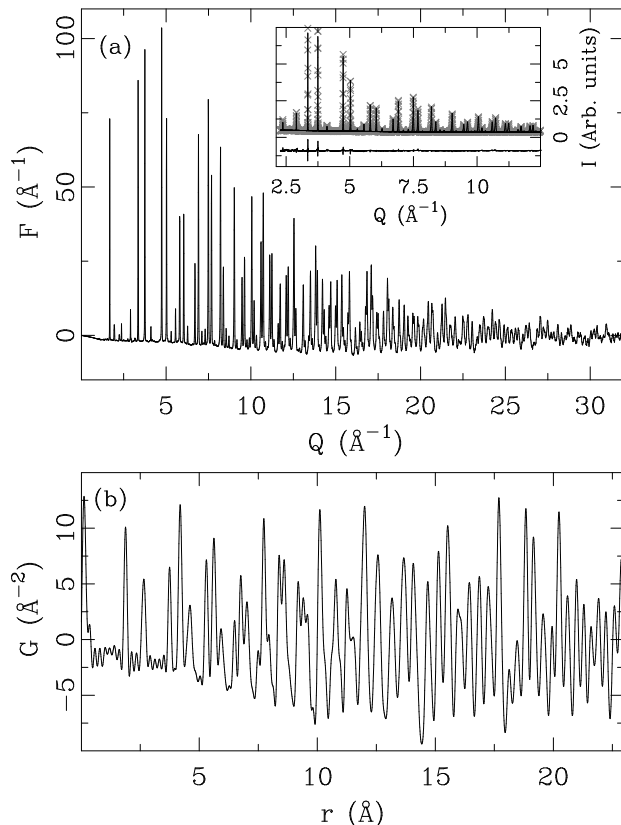


FIG. 2: Neutron experimental data of ReO_3 at 12 K and at ambient pressure: (a) reduced total scattering structure function, $F(Q)$, and (b) corresponding atomic PDF, $G(r)$. Inset shows Rietveld refinement using $\text{Pm}\bar{3}\text{m}$ model (solid line) of the normalized intensity (symbols) with the difference curve offset for clarity.

O-Re bond angle deviates from 180° by about 8° . In this newly proposed view, ReO_3 only appears cubic in the analysis of the Bragg intensities, while the local structure is suggested to be heavily distorted. In this picture the phase transition at p_c is then a tilt order-disorder transition.¹⁸ Similar conclusions were drawn from the study of XAFS spectra of antiferrodistortive perovskites $\text{Na}_{0.82}\text{K}_{0.18}\text{TaO}_3$ and NaTaO_3 .¹⁹ The results reported by Houser and Ingalls¹⁸ are in contrast to XAFS results reported earlier that suggested agreement between the local and the average structure,^{5,20,21} possibly due to the different approaches to XAFS data analysis taken in the different studies.^{18,22}

We have carried out a neutron total scattering study of ReO_3 at ambient pressure and low temperature. Based on the same data we performed both conventional Rietveld analysis, based on Bragg intensities, yielding the average crystallographic structure, and the atomic pair distribution function (PDF) analysis, which is a direct space method that includes both Bragg and diffuse scattering information, yielding structural information on local, intermediate and long range scales.^{23–25} This ap-

TABLE I: Summary of structural refinements of ReO_3 data. Atomic displacement parameters, U , are in units of \AA^2 . Derived interatomic distances d and octahedral rotation angles φ are given at the bottom. Numbers in parentheses are ESDs obtained from fitting.

| | Rietveld | $\text{Pm}\bar{3}\text{m}$ | $\text{P4}/\text{mbm}$ | $\text{Im}\bar{3}$ |
|-------------------------------------|-----------|----------------------------|------------------------|--------------------|
| a (\AA) | 3.7499(2) | 3.7508(2) | 5.3101(2) | 7.5012(3) |
| c (\AA) | - | - | 3.7430(3) | - |
| $U(\text{Re})$ | 0.0016(3) | 0.0011(1) | 0.0010(1) | 0.0010(1) |
| $x(\text{O})$ | - | - | 0.2400(6) | - |
| $y(\text{O})$ | - | - | - | 0.2520(7) |
| $z(\text{O})$ | - | - | - | 0.2417(6) |
| $U(\text{O})$ | 0.0057(5) | 0.0053(3) | 0.0031(3) | 0.0031(3) |
| $U_{\text{par}}(\text{O})$ | 0.0027(5) | 0.0026(3) | - | - |
| $U_{\text{perp}}(\text{O})$ | 0.0073(3) | 0.0061(2) | - | - |
| R_{wp} (%) | 2.97 | 7.89 | 7.87 | 8.21 |
| $d_{\text{Re-O}}$ (\AA) | 1.8749(1) | 1.8754(1) | 1.8714(1) | 1.8764(2) |
| $d_{2\text{Re-O}}$ (\AA) | - | - | 1.8789(2) | - |
| $d_{\text{1O-O}}$ (\AA) | 2.6516(1) | 2.6522(2) | 2.6520(3) | 2.6197(3) |
| $d_{2\text{O-O}}$ (\AA) | - | - | 2.6572(4) | 2.6855(3) |
| φ (deg) | 0 | 0 | 2.3(2) | 2.1(2) |

proach allows structure to be assessed on various length-scales from the same data. Our analysis rules out the existence of large local tilt amplitudes in ReO_3 .

II. EXPERIMENTAL

In this study we used 3 grams of commercially available (Sigma-Aldrich) ReO_3 sample in the form of a loose powder. Neutron time-of-flight powder diffraction measurements were carried out using the high-resolution NPDF diffractometer at the Manuel Lujan Neutron Scattering Center at Los Alamos National Laboratory. The sample was sealed in a vanadium tube with He exchange gas, and cooled down to 12 K using a closed cycle He refrigerator. Raw data were corrected for experimental effects such as sample absorption and multiple scattering using the program PDFgetN,²⁶ to obtain the total scattering structure function, $S(Q)$. This contains both Bragg and diffuse scattering and therefore information about atomic correlations on different length scales. The PDF, $G(r)$, is obtained by a Fourier transformation according to $G(r) = \frac{2}{\pi} \int_0^\infty Q[S(Q) - 1] \sin Qr dQ$, where Q is the magnitude of the scattering vector. The PDF gives the probability of finding an atom at a distance r away from another atom. The reduced total scattering structure function, $F(Q) = Q[S(Q) - 1]$, of ReO_3 at 12 K is shown in Fig. 2(a) and the resulting PDF, $G(r)$, in Fig. 2(b). PDFs refined in this study were produced using an upper limit of integration in Fourier transform Q_{max} of 32 \AA^{-1} .

The average crystal structure was verified by taking the standard Rietveld refinement approach in reciprocal space using the EXPGUI²⁷ platform operating the pro-

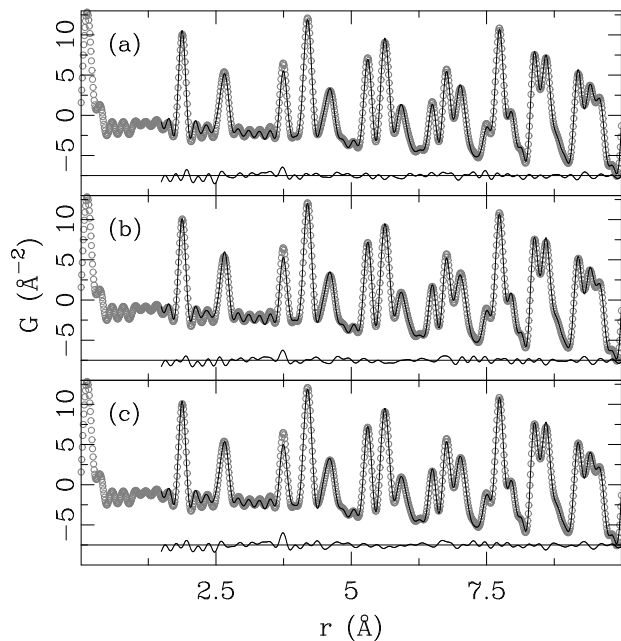


FIG. 3: Refinement of various models (solid black lines) to the 12 K neutron PDF data (open symbols): (a) $Pm\bar{3}m$ model, (b) $P4/mbm$ model, and (c) $Im\bar{3}$ model. The difference curves are offset for clarity.

gram GSAS.²⁸ The fit of the $Pm\bar{3}m$ model is shown as an inset to Fig. 2(a). The local structure was studied by refinements of structural models to the experimental PDF using the program PDFgui.²⁹ The details of the PDF method are provided elsewhere.²³

The Rietveld refinements were carried out on the ambient structure model, $Pm\bar{3}m$ space group: Re at 1a (0,0,0) and O at 3d (0.5,0,0). The PDF local structural refinements were carried out over the range 1.5-10.0 Å for three different candidate structures: conventional $Pm\bar{3}m$, and two models that allow rigid rotations of ReO_6 octahedra: $P4/mbm$ (Re at 2b (0,0,0.5), O at 2a (0,0,0) and at 4h (x,x+0.5,0.5)), and $Im\bar{3}$ (Re at 8c (0.25,0.25,0.25), O at 24g (0,y,z)).

III. RESULTS AND DISCUSSION

The results of the Rietveld refinements are shown in the inset to Fig. 2(b) and Table I. They reproduce well literature results.^{9,11-13}

We now consider the local structure measured by the PDF. The fits are shown in Fig. 3 (a)-(c), and the results summarized in Table I. The PDF does not presume any periodicity and it is therefore possible to refine lower symmetry structures than the crystallographic model where it is warranted. This may be the case when the crystal structure is an average over local domains of lower symmetry, as for example in the ferroelectric $BaTiO_3$.³⁰

As apparent from the figure, all three models provide

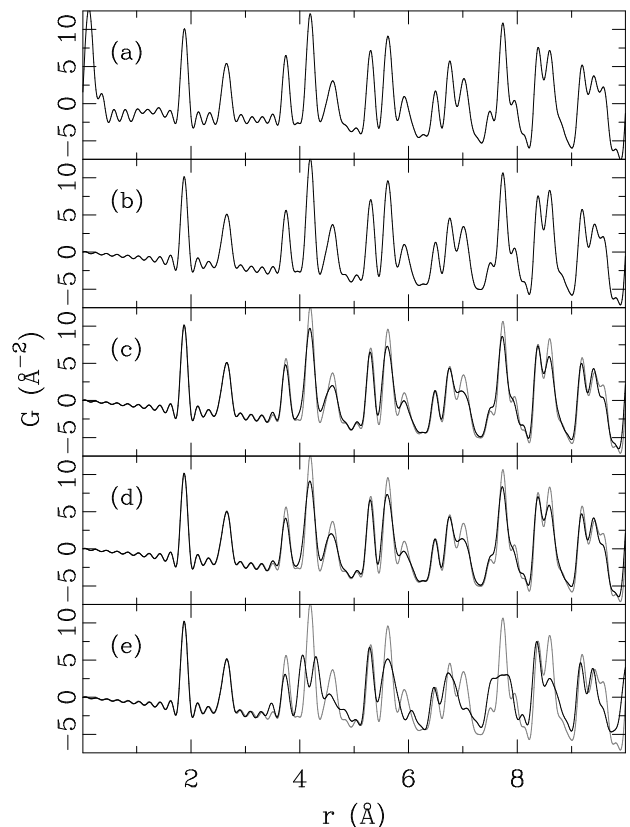


FIG. 4: Visual comparison of ReO_3 PDFs: (a) neutron PDF data, and various calculated PDFs of competing models: (b) ambient pressure $Pm\bar{3}m$, (c) 5.2 kbar $P4/mbm$, (d) 5.2 kbar $Im\bar{3}$, and (e) 7.3 kbar $Im\bar{3}$. In panels (c)-(e) gray-line PDF profile is that of $Pm\bar{3}m$ shown in panel (b), and is given for comparison. See text for details.

good fits. The fact that the crystal structure model provides a good fit with a good agreement factor suggests that there is no evidence for a lower symmetry local structure. However, as evident in the table, the good fit benefits from the model being allowed to refine anisotropic ADPs which are significantly enlarged in directions perpendicular to the Re-O bond. It is therefore interesting to consider models that allow for rotations of the octahedral units such as the symmetry lowered phases observed at high pressure. The $Im\bar{3}$ model, observed at the highest pressures, yields a quantitatively worse fit despite having more refinable parameters than the crystallographic model. On the other hand, the tetragonal $P4/mbm$ model with isotropic thermal factors imposed gives a comparable agreement to the one obtained using the crystallographic $Pm\bar{3}m$ model with anisotropic ADPs. The fits to PDF data are shown in Fig. 3(a-c) for $Pm\bar{3}m$, $P4/mbm$, and $Im\bar{3}$ models respectively, and the results are presented in Table I.

The PDF measures the instantaneous structure and it is not possible to distinguish explicitly between local tilts that are static and those that are dynamic. If the tilts

are dynamic as we presume here, the tilt angle extracted from the fits of the lower symmetry models yields an average tilt amplitude due to correlated motions of the atoms locally, i.e., rigid rotations of the octahedra, and is a useful quantitative measure of this amplitude. The octahedral rotation angles, φ ,¹³ obtained from the PDF refinements are 2.3° and 2.1° for the P4/mbm and Im $\bar{3}$ structures, respectively. These are much smaller than $\sim 4.9^\circ$ (equivalent to $\sim 8^\circ$ tilts) reported from XAFS,¹⁸ and smaller than values obtained in the pressure stabilized tilted crystal structures.¹³ PDFs calculated with the EXAFS tilt angles gave qualitatively worse fits to the data. The values refined are sufficiently small to suggest that the local tilting is coming from dynamic fluctuations of a low-energy rigid unit tilting mode, as proposed as a mechanism for the observed negative thermal expansion.^{8,31}

We have further calculated the PDFs based on data published in the literature for the three models of interest,¹³ for comparison keeping the isotropic atomic displacement parameters and the scale factor the same as those from the PDF Pm $\bar{3}$ m refinement reported here. The structural parameters were taken for cases of ambient Pm $\bar{3}$ m, 5.2 kbar P4/mbm and Im $\bar{3}$, as well as for 7.3 kbar Im $\bar{3}$ that corresponds to the stable high-pressure phase case. These calculated PDFs, and the experimental PDF profile, are shown in Fig. 4, and reveal what kind of changes are to be expected in the PDF in the case of ReO₆ octahedral rotations being present locally. At room temperature, at 5.2 kbar average octahedral rotations of 3.0° were observed, while at 7.3 kbar the rotation angle value rises to 6.6° .¹³ It is quite apparent from the calculated PDFs shown in the figure that even for a small rotation angle there are appreciable changes in the local structure, and these are rather similar for the two models that allow tilting. While the first two PDF peaks do not change at all, reflecting the rigidity of the ReO₆ octahedra,²¹ changes start to appear at higher distances as the ReO₆ network gets distorted. For a larger tilt magnitude, the changes in the local structure become much more dramatic Fig. 4(e). By visual inspection and comparison of the features seen in the calculated PDFs,

we can immediately rule out the larger tilt angle case, as there is no resemblance to the observed PDF.

IV. CONCLUSION

In summary, we used the PDF method to test a hypothesis from an earlier EXAFS study¹⁸ that the *local* rotations of ReO₆ octahedra persist in the ambient pressure, crystallographically untilted phase of ReO₃. The high-resolution neutron time-of-flight total scattering based atomic pair distribution function analysis was carried out on a dataset collected at 12 K under ambient pressure conditions. Three candidate models were tested, Pm $\bar{3}$ m, P4/mbm, and Im $\bar{3}$, and quantitative and qualitative assessment of the data were performed. No evidence was found for local octahedral rotations of a magnitude comparable to those seen in the distorted high pressure phase and beyond what might be expected from thermal and quantum zero point motion, suggesting that the local and the average structure are the same (Pm $\bar{3}$ m) as normally assumed. The PDF results shown here emphasize again the importance of using multiple complementary techniques in addressing delicate structural issues at the nanoscale.³²

Acknowledgments

ESB acknowledges useful discussions with John Provis, Efrain Rodriguez, and Anna Llobet. Work at Brookhaven National Laboratory was supported by the Office of Science, U.S. Department of Energy (OS-DOE), under contract no. DE-AC02-98CH10886. This work has benefited from the use of NPDF at the Lujan Center at Los Alamos Neutron Science Center, funded by DOE Office of Basic Energy Sciences. Los Alamos National Laboratory is operated by Los Alamos National Security LLC under DOE contract DE-AC52-06NA25396. The upgrade of NPDF has been funded by the NSF through grant DMR 00-76488.

¹ A. Ferretti, D. B. Rogers, and J. B. Goodenough, J. Phys. Chem. Solids **26**, 2007 (1965).

² C. N. King, H. C. Kirsch, and T. H. Geballe, Solid State Commun. **9**, 907 (1971).

³ P. B. Allen and W. W. Schulz, Phys. Rev. B **47**, 14434 (1993).

⁴ A. Fujimori and N. Tsuda, Solid State Commun. **34**, 433 (1980).

⁵ A. Kuzmin, J. Purans, G. Dalba, P. Fornasini, and F. Rocca, J. Phys.: Condens. Mat. **96**, 9083 (1996).

⁶ M. G. Stachiotti, F. Corà, C. R. A. Catlow, and C. O. Rodriguez, Phys. Rev. B **55**, 7508 (1997).

⁷ W. Yu, J. Zhao, and C. Jin, Phys. Rev. B **72**, 214116 (2005).

⁸ T. Chatterji, P. F. Henry, R. Mitall, and S. L. Chaplot, Phys. Rev. B **78**, 134105 (2008).

⁹ E. E. Rodriguez, A. Llobet, T. Proffen, B. C. Melot, R. Seshadri, P. B. Littlewood, and A. K. Cheetham, J. Appl. Phys. **105**, 114901 (2009).

¹⁰ F. S. Razavi, Z. Altounian, and W. R. Datars, Solid State Commun. **28**, 217 (1978).

¹¹ J. E. Schirber and B. Morosin, Phys. Rev. Lett. **42**, 1485 (1979).

¹² J. D. Axe, Y. Fujii, B. Batlogg, M. Greenblatt, and S. Di Gregorio, Phys. Rev. B **31**, 663 (1985).

¹³ J.-E. Jorgensen, J. D. Jorgensen, B. Batlogg, J. P. Reameika, and J. D. Axe, Phys. Rev. B **33**, 4793 (1986).

¹⁴ J. E. Jorgensen, W. G. Marshall, R. I. Smith, J. S. Olsen,

- and L. Gerwald, J. Appl. Crystallogr. **37**, 857 (2004).
- ¹⁵ J. E. Schirber, B. Morosin, R. W. Alkire, A. C. Larson, and P. J. Vergamini, Phys. Rev. B **29**, 4150 (1984).
 - ¹⁶ T. Chatterji and G. J. McIntyre, Solid State Commun. **139**, 12 (2006).
 - ¹⁷ K. Biswas, D. V. S. Muthu, A. K. Sood, M. B. Kruger, B. Chen, and C. N. R. Rao, J. Phys.: Condens. Mat. **19**, 436214 (2007).
 - ¹⁸ B. Houser and R. Ingalls, Phys. Rev. B **61**, 6515 (2000).
 - ¹⁹ B. Rechav, Y. Yacoby, E. A. Stern, J. J. Rehr, and M. Newville, Phys. Rev. Lett. **72**, 1352 (1994).
 - ²⁰ B. Houser, R. Ingalls, and J. J. Rehr, Physica B **208-209**, 323 (1995).
 - ²¹ G. Dalba, P. Formasini, A. Kuzmin, J. Purans, and F. Rocca, J. Phys.: Condens. Mat. **7**, 1199 (1995).
 - ²² A. Kuzmin, J. Purans, M. Benfatto, and C. R. Natoli, Phys. Rev. B **47**, 2480 (1993).
 - ²³ T. Egami and S. J. L. Billinge, *Underneath the Bragg peaks: structural analysis of complex materials*, Pergamon Press, Elsevier, Oxford, England, 2003.
 - ²⁴ S. J. L. Billinge, J. Solid State Chem. **181**, 1698 (2008).
 - ²⁵ C. A. Young and A. L. Goodwin, J. Mater. Chem. **21**, 6464 (2011).
 - ²⁶ P. F. Peterson, M. Gutmann, T. Proffen, and S. J. L. Billinge, J. Appl. Crystallogr. **33**, 1192 (2000).
 - ²⁷ B. H. Toby, J. Appl. Crystallogr. **34**, 201 (2001).
 - ²⁸ A. C. Larson and R. B. Von Dreele, General structure analysis system, Report No. LAUR-86-748, Los Alamos National Laboratory, Los Alamos, NM 87545, 1987.
 - ²⁹ C. L. Farrow, P. Juhás, J. Liu, D. Bryndin, E. S. Božin, J. Bloch, T. Proffen, and S. J. L. Billinge, J. Phys: Condens. Mat. **19**, 335219 (2007).
 - ³⁰ G. H. Kwei, S. J. L. Billinge, S.-W. Cheong, and J. G. Saxton, Ferroelectrics **164**, 57 (1995).
 - ³¹ U. Wdowik, K. Parlinski, T. Chatterji, S. Rols, and H. Schober, Phys. Rev. B **82**, 104301 (2010).
 - ³² S. J. L. Billinge and I. Levin, Science **316**, 561 (2007).